energies

MDPI

Article

Syngas Production via CO_2 Reforming of Methane over $SrNiO_3$ and $CeNiO_3$ Perovskites

Naushad Ahmad [1,*], Fahad Alharthi [1], Manawwer Alam [1], Rizwan Wahab [2], Salim Manoharadas [3] and Basel Alrayes [4]

[1] Department of Chemistry, College of Science, King Saud University, P.O. Box 2454, Riyadh 11451, Saudi Arabia; fharthi@ksu.edu.sa (F.A.); maalam@ksu.edu.sa (M.A.)
[2] Department of Zoology, College of Science, King Saud University, P.O. Box 2454, Riyadh 11451, Saudi Arabia; rwahab@ksu.edu.sa
[3] Central Laboratory, Department of Botany and Microbiology, College of Science, King Saud University, P.O. Box 2454, Riyadh 11451, Saudi Arabia; smanoharadas@ksu.edu.sa
[4] Central Laboratory, College of Science, King Saud University, P.O. Box 2454, Riyadh 11451, Saudi Arabia; bfalrayes@ksu.edu.sa
* Correspondence: anaushad@ksu.edu.sa or naushaddrnaima@gmail.com

Abstract: The development of a transition-metal-based catalyst with concomitant high activity and stability due to its distinguishing characteristics, yielding an abundance of active sites, is considered to be the bottleneck for the dry reforming of methane (DRM). This work presents the catalytic activity and durability of $SrNiO_3$ and $CeNiO_3$ perovskites for syngas production via DRM. $CeNiO_3$ exhibits a higher specific surface area, pore volume, number of reducible species, and nickel dispersion when compared to $SrNiO_3$. The catalytic activity results demonstrate higher CH_4 (54.3%) and CO_2 (64.8%) conversions for $CeNiO_3$, compared to 22% (CH_4 conversion) and 34.7% (CO_2 conversion) for $SrNiO_3$. The decrease in catalytic activity after replacing cerium with strontium is attributed to a decrease in specific surface area and pore volume, and nickel active sites covered with strontium carbonate. The stability results reveal the deactivation of both the catalysts ($SrNiO_3$ and $CeNiO_3$) but $SrNiO_3$ showed more deactivation than $CeNiO_3$, as demonstrated by deactivation factors. The catalyst deactivation is mainly attributed to carbon deposition and these findings are verified by characterizing the spent catalysts.

Keywords: perovskites; strontium; cerium; hydrogen; sintering; carbon deposition

Citation: Ahmad, N.; Alharthi, F.; Alam, M.; Wahab, R.; Manoharadas, S.; Alrayes, B. Syngas Production via CO_2 Reforming of Methane over $SrNiO_3$ and $CeNiO_3$ Perovskites. *Energies* **2021**, *14*, 2928. https://doi.org/10.3390/en14102928

Academic Editors: Wasim Khan and Giorgio Vilardi

Received: 2 April 2021
Accepted: 12 May 2021
Published: 18 May 2021

1. Introduction

Dry, or carbon dioxide reforming of methane (DRM) has gained attention in recent decades, mainly due to the fact that DRM consumes prevalent greenhouse gases i.e., methane and carbon dioxide to produce synthetic gas, which serves as an important raw material for liquid hydrocarbon formation [1–8]. Hence, DRM offers two benefits: (a) conversion of major greenhouse gases into a value-added product, and (b) the DRM product, i.e., syngas, offers equimolar H_2 and CO, which results in hydrocarbon production via Fischer–Tropsch (FT) synthesis [9–13]. The catalytic activity and stability are mainly dependent on the choice of a suitable catalyst [14]. Non-noble-metal-based catalysts, particularly transition-metal-based catalysts including catalysts of Ni, and Co, are mostly studied for DRM since these catalysts offer advantages such as their abundance, quick turnover rates, and low cost [15–18]. The bottlenecks associated with Ni-based catalysts include the loss of active metal surface area due to sintering and carbon formation during DRM which results in catalyst deactivation and also influences the selectivity of the syngas produced [19].

Generally, the basic supports or promoters, such as CeO_2, La_2O_3, and Sr^{2+}, have demonstrated better catalytic activity and enhanced chemisorption of CO_2 than acidic supports. Many researchers have reported that ceria and its modified supported catalysts

provide a promising platform for endothermic DRM processes due to their basicity, to promote CO_2 adsorption, and their high oxygen storage capacity/oxygen vacancy for CO_2 activation or the gasification of different kinds of carbon precursors [20–23]. Perovskites have shown excellent performance in catalytic and photovoltaic industries and Ni-based perovskites are favored for DRM as perovskites offer high metal dispersion and thermal stability [24,25]. The perovskites in which the B-site cation is replaced with transition metals such as Ni need to be researched in depth [26,27]. Generally, several factors contribute to the catalytic performance of a perovskite [28], (a) the choice of element(s) for B-site cation, (b) controlling vacancy and valency through the proper selection of A-site element(s) and/or partially substituting companion metal(s), (c) high dispersion obtained due to the formation of fine particles, which leads to higher specific surface area, (d) the synergy between A-site and B-site elements.

Ren et al. [29] investigated the role of an Mo_2C-Ni/ZrO_2 catalyst in the steam–CO_2 dual reformation of methane and found the catalyst exhibited high catalytic activity (~75% CH_4 conversion) and unexpected coke-resistant stability, as evidenced by TGA, even after 30 h time-on-stream. In other research, $LaBO_3$ (B = Ni, Fe, Co, and Mn) perovskites were studied for the reduction in pollution from vehicles fueled with natural gas [30]. Moreover, the effect of adding Pd to $LaBO_3$ perovskites on oxidation activity performance showed that a smaller amount of Pd contributes to improving not only lattice oxygen mobility, but also enhances the reducibility of the B-site in $LaBPd_{0.05}O_3$ perovskites. Hence, Pd addition significantly enhanced catalytic activity of the perovskites.

Messaoudi et al. [31] studied the role of bulk La_xNiO_y and supported La_xNiO_y/$MgAl_2O_4$ catalysts in DRM and found that the supported catalysts exhibited higher nickel dispersions and specific surface areas. These factors contributed to enhanced activity and stability, with minimal carbon formation during a 65 h time-on-stream. They also discovered that the supported catalysts had intact metallic nickel active sites after a long-term stability test, as verified by XRD results. The study of the impact of catalyst preparation methods, gas hourly space velocity, and reaction temperatures on catalytic performance of ternary perovskites $AZrRuO_3$ (A = Ca, Ba, and Sr) revealed that the $SrZrRuO_3$ catalyst exhibited the highest conversion and best stability among the tested perovskites [32]. Wang et al. [33] utilized perovskite (La_2O_3-$LaFeO_3$) as the support to load Ni and Co to synthesize bimetallic catalysts, to explore their performance in DRM. The loading of a suitable amount of Co increased the catalytic activity and suppressed carbon deposition, which is attributed to the crystalline structure of the perovskite.

In this work, $SrNiO_3$ and $CeNiO_3$ perovskites were synthesized and investigated for CO_2 reformation of methane. The activity performance in terms of CH_4 and CO_2 conversions and the catalyst durability, i.e., activity as function of time, are specifically elucidated herein. Overall, the aim of the study is to provide insights into the replacement of cerium with strontium and their respective responses to perovskite activity and stability under reforming conditions. The catalysts were characterized before and after activity and stability tests to understand and discuss the catalytic findings in relation to analysis results.

2. Materials and Methods

2.1. Preparation of $SrNiO_3$ and $CeNiO_3$ Nanocrystals

Nanocrystals of $SrNiO_3$ and $CeNiO_3$ were synthesized by the self-combustion method using metallic nitrates and glycine as a precursor. Firstly, 1 mmol $Ce(NO_3)_3 \cdot nH_2O$ (Sigma Aldrich, St. Louis, MO, USA—99.9%), 1 mmol $Ni(NO_3)_2 \cdot 6H_2O$ (Sigma Aldrich, St. Louis, MO, USA—99.9%), and 1 mmol $Sr(NO_3)_2$ were separately dissolved in 100 mL deionized water. The solutions of Ce/Sr and Ni were mixed in a 1:1 ratio to obtain a clear and homogeneous solution. Then, glycine (purity 99.5%), used as an ignition promoter, was added to the metal nitrate solutions (glycine:metal ions ≈ 1). The mixtures were thoroughly stirred by a magnetic mixer to eliminate the water at 60–70 °C until a homogeneous sol-like solution was formed. The gel was heated up to around 250 °C, at which temperature the ignition reaction occurred, producing a powdered precursor which still contained some

carbon residue. Finally, the powders were calcined in air at 700 °C for 6 h to eliminate the remained carbon, resulting in the formation of the perovskite structure.

2.2. Catalyst Analysis

The thermogravimetric curves (TG-DTG) of the dried precursors, from ambient temperature to 1000 °C under nitrogen flow (100 mL min^{-1}) at a heating rate of 20 °C min^{-1}, were recorded on Mettler-Toledo TGA/SDTA851e thermal analyzer, (Schwerzenbach Switzerland). All techniques mentioned below were employed on calcined powders. X-ray reflection patterns from 10–80° at a scan rate of 0.2° min^{-1} were recorded on a Shimadzu XRD-6000 diffractometer (Columbia, MD, USA) with monochromatic radiation of CuK (λ = 1.5406 Å). The specific surface area was measured by nitrogen adsorption on a Quantachrome NOVA 2000e BET system (Boynton Beach, FL, USA) and the pore size was measured by the BJH method. Temperature programmed reduction (TPR) experiments were carried out on a semiautomatic Micromeritics 2920 apparatus (Norcross, GA, USA). Samples of about 30 mg were placed in a U-shaped quartz tube, first purged in a synthetic air stream of 50 mL min^{-1} at 300 °C for 1 h and then cooled to ambient temperature. Reduction profiles were then recorded by passing a 10% H_2/Air flow over the samples at a rate of 25 mL min^{-1}, while heating at a rate of 10 °C min^{-1} from ambient temperature to 900 °C. Temperature programmed oxidation (TPO) was performed on the catalysts after the dry reforming stability tests, using the same instruments with which the TPR was performed, to verify the carbon formation. Transmission electron microscopy (TEM) was carried out using a JEOL JEM-1011 microscope (Tokyo, Japan)with an accelerating voltage of 80 kV. The samples were then placed in a copper grid where the liquid phase was evaporated. They were then used to analyze the morphology of the fresh and used catalysts for the estimation of deposited carbon.

2.3. Catalyst Activity Measurements

The dry reforming of methane was carried out in a tubular fixed-bed stainless steel reactor (i.d. 10 mm, catalytic bed length 3 mm) coupled to a gas chromatograph (Shimadzu HP5890 series II, Kyoto, Japan) with a thermal conductivity detector. The reaction conditions were: 700 °C, 0.05 g of catalyst, a gas mixture CH_4:CO_2:N_2 (30:30:10, 70 mL/min), a space velocity of 84,000 $mL{g_{cat.}}^{-1}h^{-1}$, and at 1 atm pressure. Prior to the catalytic activity tests, the catalysts were reduced in a 10% H_2/N_2 mixture (40 mL/min) at 700 °C for 120 min. Then, the H_2 flow was replaced by a He flow (60 mL/min), and the system was heated (10 °C/min) to the reaction temperature. Stability runs were carried out at 700 °C for periods of 440 min time-on-stream. The products of reactions were analyzed on-line by a VARIAN GC 3800 gas-chromatograph (Varian, Santa Clara, CA, USA), equipped with two thermal conductivity detectors and columns packed with Porapak N and 13X Molecular sieves (Varian, Santa Clara, CA, USA). The reproducibility of the gas phase composition was checked in replica experiments. In most experiments, the error was within 5%.

3. Results and Discussion

3.1. Characterization of As-Synthesized Catalysts

3.1.1. Thermal Decomposition of Precursors

Figure 1 shows the TG and DTG thermal decomposition curves of the precursors which are used to determine the final calcination temperature for the formation of crystalline products. Figure 1 shows that during the decomposition process, many phases are formed, but overall $CeNiO_3$ exhibits a two step, and $SrNiO_3$ a three step, decomposition. For $CeNiO_3$, the weight loss (~8%) started slowly at about ~75 °C, reached a maximum rate at ~150 °C (T1) and was finally completed at ~300 °C. The weight loss below this temperature was caused by the removal of the water left over from crystallization and the release of gases. The weight loss (~21%) from 300 to 550 °C with a maximum rate at 420 °C (T2 in DTG curve), may be regarded as a result of the decomposition and burning of the remaining

organic matter. Further heating caused negligible weight loss with the release of minute gaseous products in the form of CO_2 and formation of the perovskite phase.

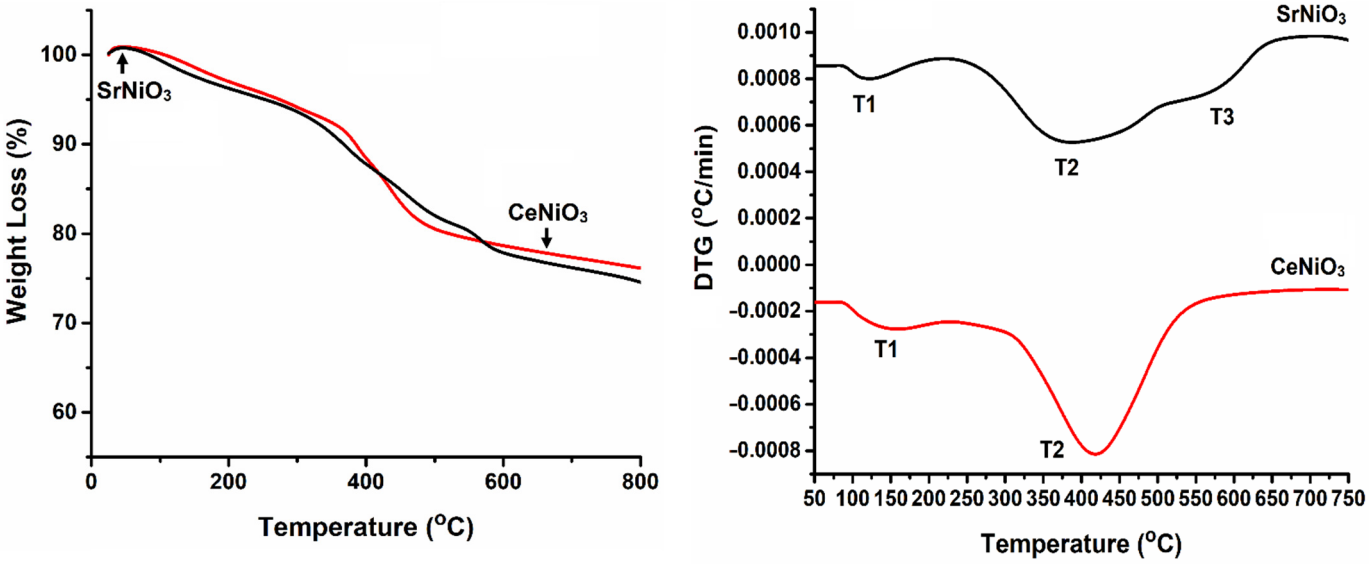

Figure 1. TG-DTG curves versus temperature of $SrNiO_3$ and $CeNiO_3$ perovskites.

On the contrary, for $SrNiO_3$, three step decomposition was observed at different intervals of temperature. The initial weight loss below 125 °C was attributed to the loss of water and some adsorbed gases. The other two steps of decomposition were attributed to the combustion of organic matter present in the precursor. Therefore, from the TG-DTG curves of the fabricated samples, it can be inferred that the perovskite phase forms above 700 °C.

3.1.2. X-ray Diffraction (XRD)

The XRD profiles of the as-synthesized $SrNiO_3$ and $CeNiO_3$ perovskites are presented in Figure 2. Upon analyzing diffraction data using MDI Jade® software (version 6.5, Materials data Inc., Newtown Square, PA, USA), it was found that diffraction peaks corresponding to 2θ values of 28.6°, 33.2°, 37.3°, 43.3°, 47.5°, 56.4°, 62.9°, 69.5°, and 76.7° are assigned to crystal planes (111), (200), (111), (200), (220), (111), and (110) of $CeNiO_3$, respectively [34,35]. The peaks appearing at 2θ = 28.6°, 33.2°, 47.5°, and 56.4° are related to cubic CeO_2 corresponding to crystal planes (111), (200), (220), and (311), respectively (JCPDS 81–0792). The peaks observed for cubic NiO were found to be at 2θ = 37.3°, 43.3°, and 62.9°, corresponding to crystal planes (111), (200), and (220), respectively (JCPDS 75–0197). Additionally, peaks ascribed to SrO and $SrCO_3$, as labelled in Figure 2, are also observed for $SrNiO_3$ perovskite [36].

3.1.3. Textural Properties

Table 1 shows the BET surface areas and pore parameters for $CeNiO_3$ and $SrNiO_3$ perovskites. The observed values of 20.7 m^2/g ($CeNiO_3$) and 12.2 m^2/g ($SrNiO_3$) are rather low and similar to those previously reported for perovskite-type oxides calcined at 800 °C, which is higher than is generally reported in the literature (below 10 m^2/g) for this type of material [37]. It is observed that the surface area of $CeNiO_3$ catalyst is higher (20.7 m^2/g) than $SrNiO_3$ catalyst (12.2 m^2/g). A similar trend is also observed for pore volume. Hence, $CeNiO_3$ is expected to show higher activity than $SrNiO_3$.

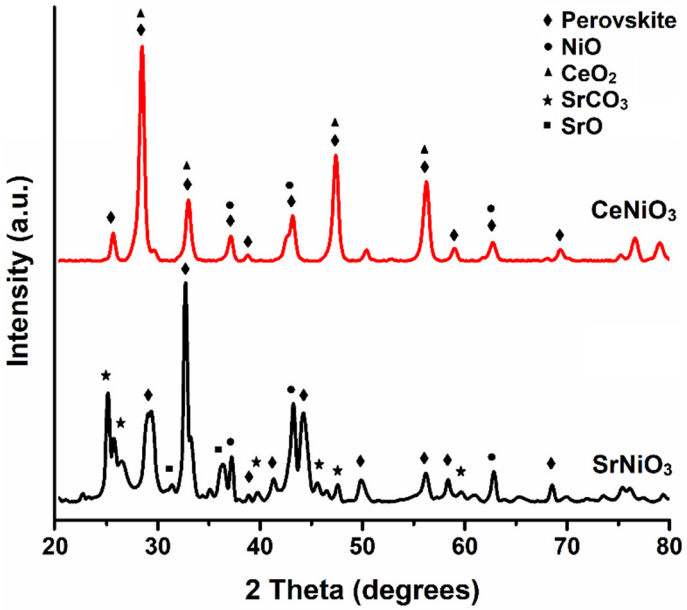

Figure 2. XRD patterns of $SrNiO_3$ and $CeNiO_3$ perovskites.

Table 1. DTG decomposition temperatures of $SrNiO_3$ and $CeNiO_3$ perovskites.

Perovskite	T1 (°C)	T2 (°C)	T3 (°C)
$CeNiO_3$	150	420	-
$SrNiO_3$	125	390	570

3.1.4. Morphological Study (TEM) of Fresh Perovskites

The morphology of as-synthesized $SrNiO_3$ and $CeNiO_3$ perovskites was analyzed by using Transmission Electron Microscopy (TEM), and microscopic images of all the fresh, reduced, and used catalysts are shown in Figure 3. The analysis of TEM images was performed using ImageJ® software (version 1.5, National Institutes of Health, Bethesda, MD, USA). The spherical particles were found to have average sizes varying from 5 to 34 nm, and 13 to 24 nm for fresh $CeNiO_3$, and $SrNiO_3$ perovskites (Figure 3a,d), respectively, which increased slightly to 8–45 nm and 16–39 nm for $CeNiO_3$, and $SrNiO_3$ perovskites (Figure 3b,e), respectively, after reduction, indicating negligible sintering after activation.

3.1.5. Temperature-Programmed Reduction (TPR)

Temperature-programmed reduction or TPR is a handy tool to analyze the reducibility–metal-support interaction and to find the reduction or activation temperature required to generate metallic particles prior to catalytic reaction. The reduction profiles shown in Figure 4 indicate the variation in reducibility and metal–support interaction when Ce is replaced with Sr. The small reduction peak, below 150 °C for the $CeNiO_3$ catalyst is related to the reduction in adsorbed oxygen species. Reduction peaks appearing between 200 and 500 °C correspond to the reduction of Ni^{3+} to Ni^{2+}, while the small shoulders at higher temperatures (>500 °C) are attributed to the reduction of Ni^{2+} to Ni^0 [38,39]. On the contrary, significant changes in the reduction peak temperatures (~245 and 345 °C) were observed for $SrNiO_3$. Additionally, the three-fold decrease in peak height of $SrNiO_3$, when compared to $CeNiO_3$, indicates that number of reducible species was suppressed by the replacement of Ce with Sr. This was also evident from the total amounts of hydrogen consumed during TPR (Table 2). The degree of reduction was significantly lower in $SrNiO_3$ (50.6%) than $CeNiO_3$ (Table 2), which can be attributed to poor dispersion of Ni within the $SrNiO_3$. The reduction in both $CeNiO_3$ and $SrNiO_3$ can be expressed as ($CeNiO_3 + H_2 \rightarrow Ni^0 + CeO_2 + H_2O$) and ($SrNiO_3 + 2H_2 \rightarrow Ni^0 + SrO + 2H_2O$). The role of these findings in influencing the catalytic activity is discussed in Section 3.

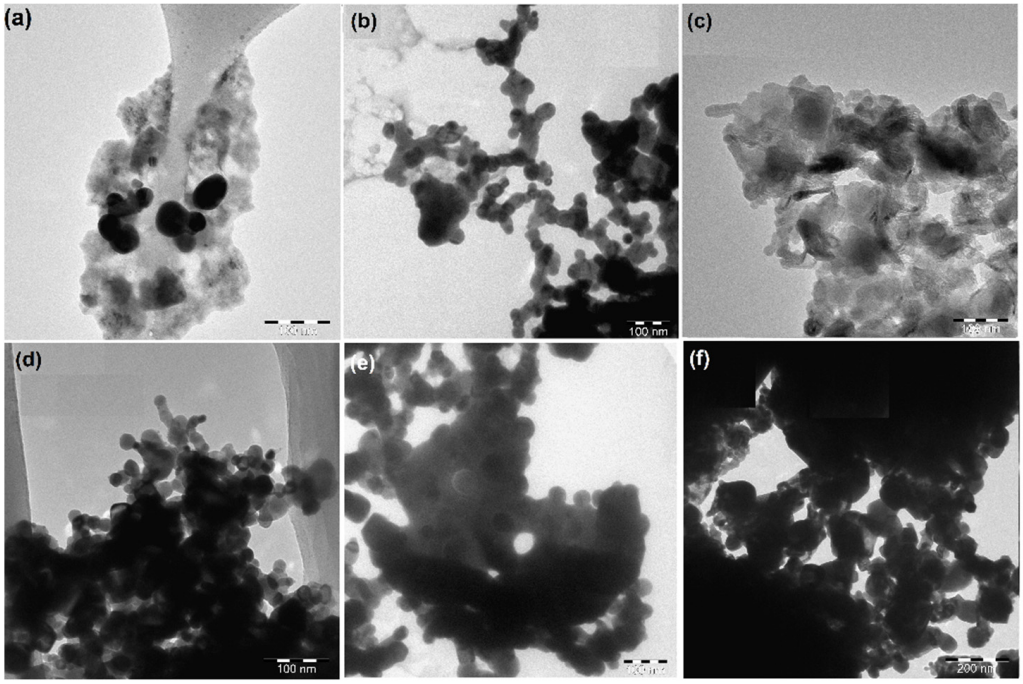

Figure 3. TEM images of (**a**) fresh $CeNiO_3$, (**b**) reduced $CeNiO_3$, (**c**) used $CeNiO_3$, (**d**) fresh $SrNiO_3$, (**e**) reduced $SrNiO_3$, and (**f**) used $SrNiO_3$.

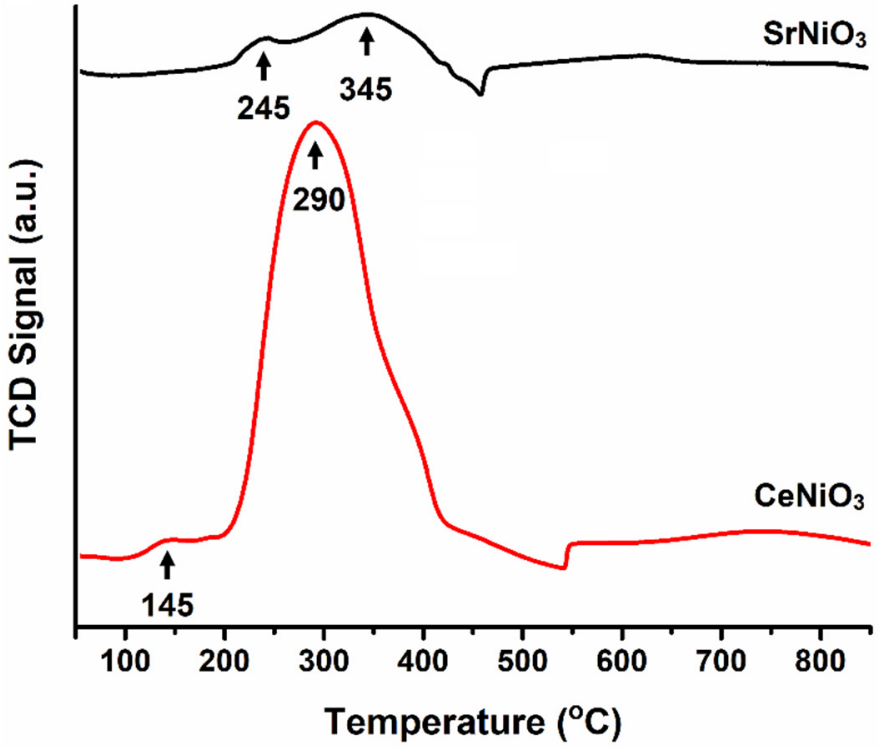

Figure 4. H_2-TPR profiles of $SrNiO_3$ and $CeNiO_3$ perovskites.

Table 2. Textural properties and deactivation factors of $SrNiO_3$ and $CeNiO_3$ perovskites.

Perovskite	S_{BET} (m^2/g)	Pore Volume (cm^3/g)	Pore Size (nm)	Deactivation Factor (%) [a]	Total Hydrogen Consumption (mmol/g) [b]	Degree of Reduction (%) [c]
$CeNiO_3$	20.7	0.162	30.1	7.7	1.11	90.5
$SrNiO_3$	12.2	0.026	9.3	64.7	0.84	50.6

[a] Deactivation Factor (D.F., %) = 100 × (CH_4 $conversion_{initial}$ − CH_4 $conversion_{final}$)/(CH_4 $conversion_{initial}$); [b] from TPR; [c] the ratio of amount of hydrogen consumed in TPR to the theoretical amount of hydrogen required to completely reduce the catalyst.

3.2. Catalytic Performances

The as-synthesized $SrNiO_3$ and $CeNiO_3$ perovskites were investigated for their catalytic performance at 700 °C. Due to the fact that the dry reforming reaction requires metallic nickel crystallites as active sites, all the perovskites were reduced under a hydrogen atmosphere prior to the reaction study. The activity results, in terms of CH_4 and CO_2 conversions as a function of time, are shown in Figure 5a,b, respectively. From Figure 5a, it is evident that $CeNiO_3$ deactivates over time, despite displaying relatively higher CH_4 conversion. $CeNiO_3$ demonstrates an initial CH_4 conversion of 54.3% which reaches 50.1% after 440 min time-on-stream, resulting in deactivation factor of 7.7% (Table 2). Strontium incorporation clearly influences CH_4 conversion, as initial conversion decreased from 54.3% ($CeNiO_3$) to 22% ($SrNiO_3$). Interestingly, significant deactivation is observed for the strontium incorporated perovskite ($SrNiO_3$) and hence a deactivation factor of 64.4% is found for $SrNiO_3$ (Table 2). The deactivation of the catalysts and the factors behind it are analyzed by characterizing the spent catalysts, as discussed in Section 3.3. A similar trend was found in Figure 5b for CO_2 conversions versus time-on-stream. Initial CO_2 conversions of 64.8 and 34.7% were demonstrated by $CeNiO_3$ and $SrNiO_3$, respectively, which reached final conversions of 58 and 11.5%, respectively. It is also worth observing from Figure 5 that CO_2 conversions are higher than those of CH_4. This result implies the simultaneous existence of the reverse water-gas shift reaction ($CO_2 + H_2 \rightarrow CO + H_2O$) that generates H_2/CO molar ratios lower than the stoichiometric one ($H_2/CO = 1.0$) due to the fact that hydrogen consumes CO_2 and CO in a disproportionation or Boudouard reaction ($2CO \rightarrow CO_2 + C$). A separate section is dedicated to the discussion of catalytic activity results in relation to their analysis findings in Section 3.4.

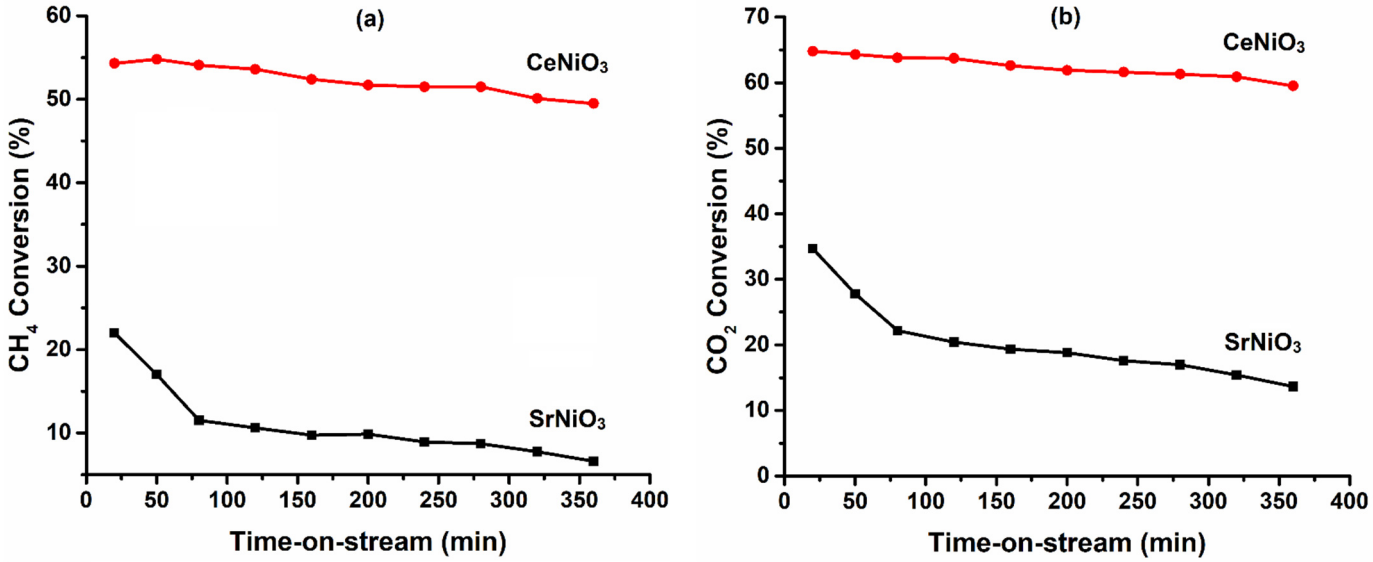

Figure 5. (**a**) CH_4 conversion, and (**b**) CO_2 conversion versus time-on-stream (TOS) of $SrNiO_3$ and $CeNiO_3$ perovskites.

3.3. Characterization of Spent Perovskites

The perovskites, after being investigated for dry reforming reaction, were further analyzed to understand their catalytic performance results. $CeNiO_3$ showed deactivation while all the perovskites showed CO_2 conversions higher than CH_4 conversions (Figure 5), which gave rise to side reactions such as reverse water-gas shift and CO disproportionation. The perovskites were then analyzed using temperature-programmed oxidation and transition electron microscope to assess the modifications to perovskites during reaction.

3.3.1. Temperature-Programmed Oxidation (TPO)

In order to verify the possibility of carbon deposition over the surface of the perovskites, TPO analysis was carried out after the reforming reaction. Figure 6 presents the TPO results of the $SrNiO_3$ and $CeNiO_3$ perovskites. Both of the perovskites showed one broad peak in the temperature range of from 170 to 550 °C. The peak maximum temperatures are ~320 and 335 °C for $SrNiO_3$ and $CeNiO_3$, respectively. These peaks were attributed to the polymeric species of carbon deposited and/or less reactive surface carbides formed during the reaction, as reported earlier [40,41]. The peak temperatures correspond to the degree of hydrogenation of surface carbon species and the surface carbon changing to be graphitic in nature as the peak temperature increased. It is evident from peak temperatures that both perovskites have shown the formation of mainly polymeric carbon species and that their interaction with the catalyst surface changes, becoming stronger with strontium replacement by cerium, as demonstrated by the increase in peak temperatures from 320 to 335 °C. It could also be observed that cerium oxide played a role in controlling the carbon deposition, carbon alleviation and the degree of interaction between carbon and the catalyst surface.

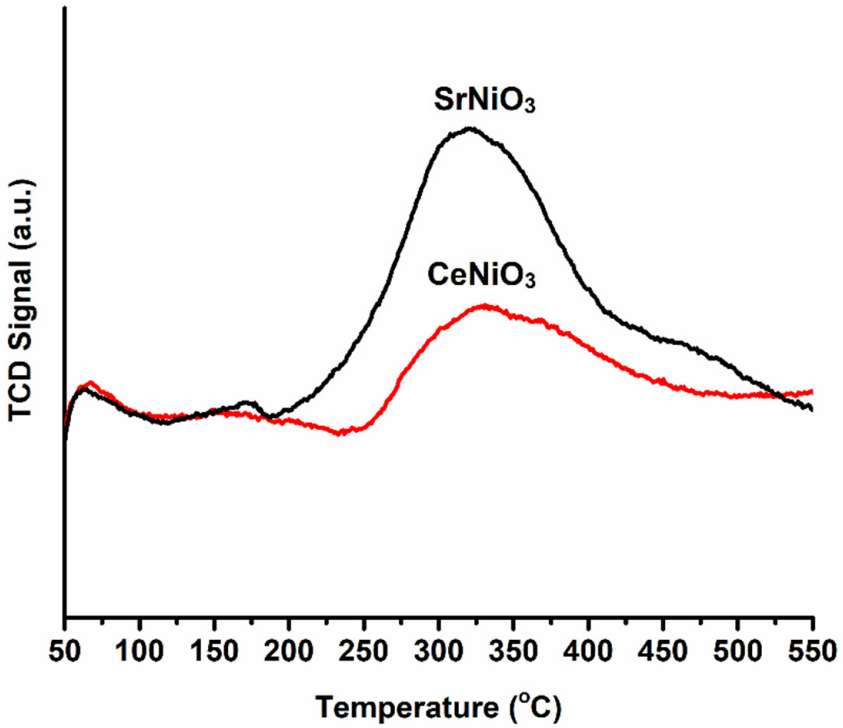

Figure 6. TPO profiles of $SNiO_3$ and $CeNiO_3$ perovskites.

3.3.2. Transition Electron Microscopy (TEM)

To further verify the causes of deactivation or modification of the perovskites during the reforming reaction, transition electron microscopic analysis was carried out. The TEM images in Figure 3c,f show particle sizes of 10–70 nm and 25–77 nm for $CeNiO_3$ and $SrNiO_3$ spent catalysts, respectively. The TEM results manifest the formation of carbon over spent

catalysts as well as noticeable agglomeration of the perovskite particles. Hence, sintering also contributes to the deactivation of $SrNiO_3$ and $CeNiO_3$. These findings are discussed below in Section 3.4.

3.4. Discussion

The as-synthesized perovskites were analyzed prior to reaction to predict their performance during reaction. TG-DTG data show that the precursors were converted into perovskite after being calcined at the temperatures demonstrated by the DTGs (Figure 1 and Table 1). Both $SrNiO_3$ and $CeNiO_3$ perovskites were formed when they were calcined at 700 °C. XRD diffraction patterns (Figure 2) have shown the existence of perovskite structure and oxides of nickel and cerium along with oxide and carbides of strontium. The textural properties (Table 2), analyzed using nitrogen adsorption-desorption isotherms, demonstrated specific surface areas of 12.2 and 20.7 m^2/g ($SrNiO_3$ and $CeNiO_3$, respectively). Morphological analysis using TEM (Figure 3) displayed spherical particles with different sizes as strontium is replaced with cerium. The TPR profiles (Figure 4) aimed to find out the reduction behavior of the perovskites and it was evident that the reduction in oxides of nickel was easier for $CeNiO_3$, while it became difficult in the case of $SrNiO_3$ which is in agreement with the TG-DTG results (Figure 1). Based on the analyses of perovskites prior to the reforming reaction, it was inferred that $CeNiO_3$ exhibited a higher specific surface area, number of reducible species, and a wider range of particle sizes in comparison with $SrNiO_3$. Hence, CeNiO3 perovskite was expected to show higher activity which was evidenced by CH_4 and CO_2 conversions (Figure 5). It is well known that the dry reforming reaction mechanism needs adsorption of reactants on the active sites, which then dissociate and react to give products, followed by product desorption [4]. Metallic nickel is the main active site for CH_4 adsorption. From catalyst activity results, it was found that $SrNiO_3$ showed a decrease in both CH_4 and CO_2 conversions which can be attributed to the loss of nickel active sites due to agglomeration during calcination, and/or the covering of nickel with strontium oxide or carbonate. From the TPR and TEM images, it can be seen that $SrNiO_3$ has higher reduction temperatures and there is evidence of sintering during calcination. Similarly, the XRD patterns show that clear peaks of oxides and carbonates of strontium are found for $SrNiO_3$ perovskite, which supports the hypothesis that nickel active sites are covered.

Figure 5 also shows the activity results as a function of reaction time which is associated with the durability of the perovskites. It is evident that both perovskites showed deactivation over time, which can be attributed to both sintering and carbon deposition, as evidenced by the TPO and TEM images of the spent catalysts. The extent of the sintering is almost the same for both perovskites during DRM. This suggests that the carbon deposition resulted from methane decomposition, which is a prevalent side reaction at high reaction temperatures and is considered to be the main cause of deactivation. This is in agreement with the TPO results, where it is evident that carbon gasification over the surface of $CeNiO_3$ requires a higher temperature when compared to $SrNiO_3$. Moreover, CO_2 conversions for $CeNiO_3$ are higher than for $SrNiO_3$ which implies that the oxidative environment suitable for carbon gasification is predominant in $CeNiO_3$, suggesting easier carbon removal and no deactivation in this catalyst. Rynkowski et al. [42] investigated DRM in reduced $La_{2-x}Sr_xNiO_4$ perovskite oxides and concluded that the smaller amounts of strontium exhibited less activity and more stability when compared to strontium-free catalysts. Choudhary et al. [43] also studied the influence of the partial substitution of La and Ni in $LaNiO_3$ perovskites and found that catalytic activity is lost after La is partially substituted by Sr in $LaNiO_3$ perovskite.

4. Conclusions

This study investigated the activity and stability performance of $SrNiO_3$ and $CeNiO_3$ perovskites for DRM. The analysis results of $CeNiO_3$ prior to the reaction revealed well-dispersed nickel nanoparticles over the catalyst's surface, enhanced number of reducible

species, and higher specific surface areas and pore volumes, which remained key factors in influencing both catalytic activity and durability. The $CeNiO_3$ perovskite demonstrated higher CH_4 and CO_2 conversions as compared to $SrNiO_3$ but both perovskites deactivated over time. Lower activity in the case of $SrNiO_3$ reveals the fact that nickel active sites are covered with strontium carbonates, which is in agreement with previously reported results. The analyses of the perovskites after reaction assisted in locating the cause of deactivation. Though all perovskites showed significant sintering, it was not considered to be the main cause of deactivation as $SrNiO_3$ showed more deactivation despite a similar extent of sintering. Hence, carbon deposition, as evidenced by the TEM and TPO images of spent perovskites, was the main deactivation factor. The investigation of recyclability, reactivation of the developed catalyst system, and the role of strontium combined with Ce-based perovskites are planned for future work.

Author Contributions: N.A., F.A., and M.A. synthesized the catalysts, carried out all the experiments and characterization tests, and wrote the manuscript. R.W., B.A., and S.M. prepared the catalyst and contributed to proofreading of the manuscript. N.A. and F.A. contributed to the analysis of the data and the writing and review of the manuscript. All authors have read and agreed to the published version of the manuscript.

Funding: This research was funded by King Saud University under NPST project (14-PET851-02).

Institutional Review Board Statement: Not Applicable.

Informed Consent Statement: Not Applicable.

Data Availability Statement: Not Applicable.

Acknowledgments: The authors would like to extend their sincere appreciation to the King Saud University for its funding to this NPST project (14-PET851-02).

Conflicts of Interest: The authors declare no conflict of interest.

References

1. Wang, Y.; Yao, L.; Wang, S.; Mao, D.; Hu, C. Low-temperature catalytic CO_2 dry reforming of methane on Ni-based catalysts: A review. *Fuel Process. Technol.* **2018**, *169*, 199–206. [CrossRef]
2. Li, H.; He, Y.; Shen, D.; Cheng, S.; Wang, J.; Liu, H.; Xing, C.; Shan, S.; Lu, C.; Yang, R. Design an in-situ reduction of Ni/C-SiO_2 catalyst and new insight into pretreatment effect for CH_4–CO_2 reforming reaction. *Int. J. Hydrogen Energy* **2017**, *42*, 10844–10853. [CrossRef]
3. Al-Fatesh, A.S.; Arafat, Y.; Atia, H.; Ibrahim, A.A.; Ha, Q.L.M.; Schneider, M.; M-Pohl, M.; Fakeeha, A.H. CO_2-reforming of methane to produce syngas over Co-Ni/SBA-15 catalyst: Effect of support modifiers (Mg, La and Sc) on catalytic stability. *J. CO2 Util.* **2017**, *21*, 395–404. [CrossRef]
4. Ibrahim, A.A.; Fakeeha, A.H.; Al-Fatesh, A.S. Enhancing hydrogen production by dry reforming process with strontium promoter. *Int. J. Hydrogen Energy* **2014**, *39*, 1680–1687. [CrossRef]
5. Li, D.; Lu, M.; Xu, S.; Chen, C.; Zhan, Y.; Jiang, L. Preparation of supported Co catalysts from Co-Mg-Al layered double hydroxides for carbon dioxide reforming of methane. *Int. J. Hydrogen Energy* **2017**, *42*, 5063–5071. [CrossRef]
6. Al-Fatesh, A.S.; Arafat, Y.; Ibrahim, A.A.; Atia, H.; Fakeeha, A.H.; Armbruster, U.; Abasaeed, A.E.; Frusteri, F. Evaluation of Co-Ni/Sc-SBA–15 as a novel coke resistant catalyst for syngas production via CO_2 reforming of methane. *Appl. Catal. A Gen.* **2018**, *567*, 102–111. [CrossRef]
7. Djinovic, P.; Batista, J.; Pintar, A. Efficient catalytic abatement of greenhouse gases: Methane reforming with CO_2 using a novel and thermally stable Rh-CeO_2 catalyst. *Int. J. Hydrogen Energy* **2012**, *37*, 2699–2707. [CrossRef]
8. El Hassan, N.; Kaydouh, M.N.; Geagea, H.; El Zein, H.; Jabbour, K.; Casale, S.; El Zakhem, H.; Massiani, P. Low temperature dry reforming of methane on rhodium and cobalt based catalysts: Active phase stabilization by confinement in mesoporous SBA-15. *Appl. Catal. A Gen.* **2016**, *520*, 114–121. [CrossRef]
9. Khan, W.U.; Li, X.; Baharudin, L.; Yip, A.C.K. Copper-promoted cobalt/titania nanorod catalyst for CO hydrogenation to hydrocarbons. *Catal. Lett.* **2021**, in press. [CrossRef]
10. Khan, W.U.; Baharudin, L.; Choi, J.; Yip, A.C.K. Recent progress in CO hydrogenation over bimetallic catalysts for higher alcohol synthesis. *ChemCatChem* **2020**, *13*, 533–542. [CrossRef]
11. Khan, W.U.; Chen, S.S.; Tsang, D.C.W.; Hu, X.; Lam, F.L.Y.; Yip, A.C.K. Catalytically active interfaces in titania nanorod-supported copper catalysts for CO oxidation. *Nano Res.* **2021**, *13*, 111–120. [CrossRef]
12. Horn, R.; Schlögl, R. Methane activation by heterogeneous catalysis. *Catal. Lett.* **2015**, *45*, 23–39. [CrossRef]

13. Rostrup-Nielsen, J.R.; Sehested, J.; Nørskov, J.K. Hydrogen and synthesis gas by steam- and CO_2 reforming. *Adv. Catal.* **2002**, *47*, 65–139. [CrossRef]
14. Kang, D.; Yu, J.; Ma, W.; Zheng, M.; He, Y.; Li, P. Synthesis of Cu/Ni-$La_{0.7}Sr_{0.3}Cr_{0.5}Mn_{0.5}O_{3-\delta}$ and its catalytic performance on dry methane reforming. *J. Rare Earth* **2019**, *37*, 585–593. [CrossRef]
15. Chein, R.Y.; Fung, W.Y. Syngas production via dry reforming of methane over CeO_2 modified Ni/Al_2O_3 catalysts. *Int. J. Hydrogen Energy* **2019**, *44*, 14303–14315. [CrossRef]
16. Ma, Q.; Guo, L.; Fang, Y.; Li, H.; Zhang, J.; Zhao, T.S.; Yang, G.; Yoneyam, Y.; Tsubaki, N. Combined methane dry reforming and methane partial oxidization for syngas production over high dispersion Ni based mesoporous catalyst. *Fuel Process. Technol.* **2019**, *188*, 98–104. [CrossRef]
17. Abdullah, B.; Ghani, N.A.A.; Vo, D.V.N. Recent advances in dry reforming of methane over Ni-based catalysts. *J. Clean. Prod.* **2017**, *162*, 170–185. [CrossRef]
18. Ali, S.; Khader, M.M.; Almarri, M.J.; Abdelmoneim, A.G. Ni-based nano-catalysts for the dry reforming of methane. *Catal. Today* **2020**, *343*, 26–37. [CrossRef]
19. Shen, J.; Reule, A.A.C.; Semagina, N. Ni/$MgAl_2O_4$ catalyst for low-temperature oxidative dry methane reforming with CO_2. *Int. J. Hydrogen Energy* **2019**, *44*, 4616–4629. [CrossRef]
20. Wang, F.; Han, K.; Yu, W.; Zhao, L.; Wang, Y.; Wang, X.; Yu, H.; Shi, W. Low temperature CO_2 reforming with methane reaction over CeO_2-modified Ni@SiO_2 catalysts. *ACS Appl. Mater. Interf.* **2020**, *12*, 35022–35034. [CrossRef] [PubMed]
21. Han, K.; Yu, W.; Xu, L.; Deng, Z.; Yu, H.; Wang, F. Reducing carbon deposition and enhancing reaction stability by ceria for methane dry reforming over Ni@SiO_2@CeO_2 catalyst. *Fuel* **2021**, *291*, 120182. [CrossRef]
22. Charisiou, N.D.; Siakavelas, G.; Papageridis, K.N.; Baklavaridis, A.; Tzounis, L.; Avraam, D.G.; Goula, M.A. Syngas production via the biogas dry reforming reaction over nickel supported on modified with CeO_2 and/or La_2O_3 alumina catalysts. *J. Nat. Gas. Sci. Eng.* **2016**, *31*, 164–183. [CrossRef]
23. Goula, M.A.; Charisiou, N.D.; Siakavelas, G.; Tzounis, L.; Tsiaoussis, I.; Panagiotopoulou, P.; Goula, G.; Yentekakis, I.V. Syngas production via the biogas dry reforming reaction over Ni supported on zirconia modified with CeO_2 or La_2O_3 catalysts. *Int. J. Hydrogen Energy* **2017**, *42*, 13724–13740. [CrossRef]
24. Liu, M.; Zhang, H.; Gedamu, D.; Fourmont, P.; Rekola, H.; Hiltunen, A.; Cloutier, S.G.; Nechache, R.; Priimagi, A.; Vivo, P. Halide perovskite nanocrystals for next-generation optoelectronics. *Small* **2019**, *15*, 1900801. [CrossRef]
25. Zhang, H.; Deng, R.; Wang, J.; Li, X.; Chen, Y.-M.; Liu, K.; Taubert, C.J.; Cheng, S.Z.D.; Zhu, X. Crystalline organic pigment-based field-effect transistors. *ACS Appl. Mater. Interf.* **2017**, *9*, 21891–21899. [CrossRef]
26. Khalesi, A.; Arandiyan, H.R.; Parvari, M. Production of Syngas by CO_2 Reforming on $M_xLa_{1-x}Ni_{0.3}Al_{0.7}O_{3-d}$ (M = Li, Na, K). *Ind. Eng. Chem. Res.* **2008**, *47*, 5892–5898. [CrossRef]
27. Pérez-Camacho, M.N.; Abu-Dahrieh, J.; Goguet, A.; Sun, K.; Rooney, D. Self-cleaning perovskite-type catalysts for the dry reforming of methane. *Chin. J. Catal.* **2014**, *35*, 1337–1346. [CrossRef]
28. Voorhoeve, R.J.H. 5—Perovskite-related oxides as oxidation—Reduction catalysts. In *Advanced Materials in Catalysis*; Burton, J.J., Garten, R.L., Eds.; Academic Press: New York, NY, USA, 1977; pp. 129–180.
29. Ren, P.; Zhao, Z. Unexpected coke-resistant stability in steam-CO_2 dual reforming of methane over the robust Mo_2C-Ni/ZrO_2 catalyst. *Catal. Commun.* **2019**, *119*, 71–75. [CrossRef]
30. Ziaei-Azad, H.; Khodadadi, A.; Esmaeilnejad-Ahranjani, P.; Mortazavi, Y. Effects of Pd on enhancement of oxidation activity of $LaBO_3$ (B = Mn, Fe, Co and Ni) pervoskite catalysts for pollution abatement from natural gas fueled vehicles. *Appl. Catal. B Environ.* **2011**, *102*, 62–70. [CrossRef]
31. Messaoudi, H.; Thomas, S.; Djaidja, A.; Slyemi, S.; Barama, A. Study of La_xNiO_y and La_xNiO_y/$MgAl_2O_4$ catalysts in dry reforming of methane. *J. CO2 Util.* **2018**, *24*, 40–49. [CrossRef]
32. Ruocco, C.; Caprariis, B.D.; Palma, V.; Petrullo, A.; Ricca, A.; Scarsella, M.; Filippis, P.D. Methane dry reforming on Ru perovskites, $AZrRuO_3$: Influence of preparation method and substitution of A cation with alkaline earth metals. *J. CO2 Util.* **2019**, *30*, 222–231. [CrossRef]
33. Wang, H.; Dong, X.; Zhao, T.; Yu, H.; Li, M. Dry reforming of methane over bimetallic Ni-Co catalyst prepared from La$(Co_xNi_{1-x})_{0.5}Fe_{0.5}O_3$ perovskite precursor: Catalytic activity and coking resistance. *Appl. Catal. B Environ.* **2009**, *245*, 302–313. [CrossRef]
34. Dehghani, F.; Ayatollahi, S.; Bahadorikhalili, S.; Esmaeilpour, M. Synthesis and characterization of mixed–metal oxide nanoparticles ($CeNiO_3$, $CeZrO_4$, $CeCaO_3$) and application in adsorption and catalytic oxidation–decomposition of asphaltenes with different chemical structures. *Pet. Chem.* **2020**, *60*, 731–743. [CrossRef]
35. Harikrishnan, M.P.; Mary, A.J.C.; Bose, A.C. Electrochemical performance of $ANiO_3$ (A = La, Ce) perovskite oxide material and its device performance for supercapattery application. *Electrochim. Acta* **2020**, *362*, 137095. [CrossRef]
36. García de la Cruz, R.M.; Falcón, H.; Peña, M.A.; Fierro, J.L.G. Role of bulk and surface structures of $La_{1-x}Sr_xNiO_3$ perovskite-type oxides in methane combustion. *Appl. Catal. B Environ.* **2001**, *33*, 45–55. [CrossRef]
37. Wang, Y.; Cui, X.; Li, Y.; Shu, Z.; Chen, H.; Shi, J. A simple co-nanocasting method to synthesize high surface area mesoporous $LaCoO_3$ oxides for CO and NO oxidations. *Microporous Mesoporous Mater.* **2013**, *176*, 8–15. [CrossRef]

38. Wei, Y.; Zhao, Z.; Jiao, J.; Liu, J.; Duan, A.; Jiang, G. Facile synthesis of three-dimensionally ordered macroporous $LaFeO_3$-supported gold nanoparticle catalysts with high catalytic activity and stability for soot combustion. *Catal. Today* **2015**, *245*, 37–45. [CrossRef]
39. Chen, J.; He, Z.; Li, G.; An, T.; Shi, H.; Li, Y. Visible-light-enhanced photothermocatalytic activity of ABO_3-type perovskites for the decontamination of gaseous styrene. *Appl. Catal. B Environ.* **2017**, *209*, 146–154. [CrossRef]
40. Moral, A.; Reyero, I.; Alfaro, C.; Bimbela, F.; Gandía, L.M. Syngas production by means of biogas catalytic partial oxidation and dry reforming using Rh-based catalysts. *Catal. Today* **2018**, *299*, 280–288. [CrossRef]
41. Verykios, X. Mechanistic aspects of the reaction of CO_2 reforming of methane over Rh/Al_2O_3 catalyst. *Appl. Catal. A. Gen.* **2003**, *255*, 101–111. [CrossRef]
42. Rynkowski, J.; Samulkiewicz, P.; Ladavos, A.K.; Pomonis, P.J. Catalytic performance of reduced $La_{2-x}Sr_xNiO_4$ perovskite-like oxides for CO_2 reforming of CH_4. *Appl. Catal. A Gen.* **2004**, *263*, 1–9. [CrossRef]
43. Choudhary, V.R.; Uphade, B.S.; Belhekar, A.A. Oxidative conversion of methane to syngas over $LaNiO_3$ perovskite with or without simultaneous steam and CO_2 reforming reactions: Influence of partial substitution of La and Ni. *J. Catal.* **1996**, *163*, 312–318. [CrossRef]